THE JOURNAL OF BIOLOGICAL CHEMISTRY VOL. 289, NO. 41, pp. 28087–28093, October 10, 2014

Stu2, the Budding Yeast XMAP215/Dis1 Homolog, Promotes Assembly of Yeast Microtubules by Increasing Growth Rate and Decreasing Catastrophe Frequency*

Received for publication, May 23, 2014, and in revised form, August 25, 2014 Published, JBC Papers in Press, August 29, 2014, DOI 10.1074/jbc.M114.584300

Marija Podolski, Mohammed Mahamdeh, and Jonathon Howard[1]

From the Department of Molecular Biophysics and Biochemistry, Yale University, New Haven, Connecticut 06520

Background: The reported inhibition of microtubule growth by Stu2 is difficult to reconcile with its cellular phenotypes.
Results: Using microscopy assays, we found that Stu2 increases the growth rate and decreases the catastrophe frequency of yeast microtubules.
Conclusion: Stu2 promotes microtubule growth, with considerably higher activity on budding yeast microtubules.
Significance: The biochemical properties of Stu2 reported here account for the mitotic phenotypes observed in cells.

Stu2 is the budding yeast member of the XMAP215/Dis1 family of microtubule polymerases. It is essential in cell division, allowing proper spindle orientation and metaphase chromosome alignment, as well as spindle elongation during anaphase. Despite Stu2 having a phenotype that suggests it promotes microtubule growth, like the other members of the XMAP215/Dis1 family, previous studies with purified Stu2 indicate only that it antagonizes microtubule growth. One potential explanation for these contradictory findings is that the assays were performed with mammalian brain tubulin, which may not be the right substrate to test the activity of Stu2 given that yeast and brain tubulins are quite divergent in sequence and that the vertebrate tubulins are subject to many post-translational modifications. To test this possibility, we reconstituted the activity of Stu2 with purified budding yeast tubulin. We found that Stu2 accelerated microtubule growth in yeast tubulin by severalfold, similar to the acceleration reported for XMAP215 in porcine brain tubulin. Furthermore, Stu2 accelerated polymerization in yeast tubulin to a much greater extent than in porcine brain tubulin, and the concentration of Stu2 required to reach 50% maximum activity in yeast tubulin was nearly 2 orders of magnitude lower than that in porcine brain tubulin. We conclude that Stu2 is a microtubule polymerase, like its relatives, and that its activity is considerably higher in yeast tubulin compared with mammalian brain tubulin. The biochemical properties of Stu2 reported here account for many of the phenotypes of Stu2 observed in cells.

Microtubules, cytoskeletal filaments composed of α,β-tubulin heterodimers, serve as tracks for molecular motors and provide structure to organelles such as mitotic spindles and axonemes (1, 2). The growth and shrinkage of microtubules are regulated by microtubule-associated proteins (MAPs)[2] that can increase or decrease the rate of polymerization or depolymerization or that can regulate the switching between growth and shrinkage (3–5). This study addresses the protein Stu2, a member of the XMAP215/Dis1 family of microtubule polymerases, which, unexpectedly and unlike other members of the family, has been reported to inhibit, rather than accelerate, polymerization.

Members of the XMAP215/Dis1 family promote microtubule growth both in cells and in biochemical assays with purified proteins (6). The founding member of this family, XMAP215, is required for rapid microtubule growth in *Xenopus laevis* egg extracts and accelerates elongation of the fast-growing plus ends of microtubules by up to 8-fold in the presence of purified bovine brain tubulin (7). Tea1, the *Aspergillus nidulans* homolog of XMAP215, accelerates the growth of porcine brain microtubules to a similar extent as XMAP215 (8). Stu2, the budding yeast homolog of this family, is required for elongation of the mitotic spindle during anaphase (9), as well as for spindle orientation and metaphase chromosome alignment (10). Mutants lacking the TOG1 domain of Stu2 exhibit shorter cytoplasmic microtubules and shorter spindles (11), consistent with Stu2 promoting microtubule growth. However, studies with purified Stu2 have shown that it slows, rather than accelerates, elongation of microtubules grown in brain tubulin (12). Furthermore, these authors reported that Stu2 also promotes catastrophe, the transition of growing microtubules to shrinking ones, which often correlates with slower growth rates. One interpretation of these results is that not all members of the XMAP215/Dis1 family are polymerases and that the shared protein domains, notably the TOG domains (13, 14), may have divergent activities.

An alternative explanation for the difference in Stu2 and XMAP215 activities is that mammalian brain tubulin may not be the right substrate to test the activity of Stu2 given that yeast

* This work was supported by National Institutes of Health Grant R01 GM110386 (to J. H.).
[1] To whom correspondence should be addressed: Dept. of Molecular Biophysics and Biochemistry, Yale University, 266 Whitney Ave., New Haven, CT 06511. Tel.: 203-432-7245; Fax: 203-432-8492; E-mail: jonathon.howard@yale.edu.

[2] The abbreviations used are: MAP, microtubule-associated protein; GMP-CPP, guanosine 5′-(α,β-methyleno)triphosphate; DIC, differential interference contrast.

and brain tubulins are quite divergent in sequence and that the vertebrate tubulins are subject to many post-translational modifications (see "Discussion"). To test this possibility, we reconstituted the polymerization activity of Stu2 with budding yeast tubulin.

EXPERIMENTAL PROCEDURES

Protein Expression, Purification, and Labeling—We used two Stu2 constructs: the N-terminally His_6-tagged full-length protein (Stu2) and the same protein with C-terminal spacer (AAEFM) followed by enhanced GFP (Stu2-GFP). Sf^+ cells were transfected with the baculovirus encoding Stu2 or Stu2-GFP and harvested by centrifugation at 1300 rpm for 15 min. The pellets were dissolved in cold lysis buffer (50 mM HEPES (pH 7.5), 150 mM NaCl, 5% glycerol, 0.1% Tween 20, 1.5 mM $MgCl_2$, 3 mM EGTA, 1 mM DTT, 0.5 mM MgATP, and protease inhibitors (1 mM PMSF, 10 μg/ml antipain, 5 μg/ml chymotrypsin, 20 μg/ml as L-1-tosylamido-2-phenylethyl chloromethyl ketone, 2 μg/ml aprotinin, 0.7 μg/ml pepstatin A, 0.5 μg/ml leupeptin, 20 μg/ml TAME (*N*-p-Tosyl-L-arginine methyl ester hydrochloride), 1 mM benzamidine, and 10 μM E64)). Normally, 4 ml of lysis buffer was used per 1 g of pellet. The crude lysate was clarified by centrifugation at 13,000 × *g* for 20 min and loaded onto an SP-Sepharose column (Amersham Biosciences HiTrap SP HP). The column was washed with cation buffer (6.7 mM HEPES, 6.7 mM MES, 6.7 mM NaOAc (pH 7.2), 150 mM NaCl, 1.5 mM $MgCl_2$, 1 mM DTT, 10 μM MgATP, and protease inhibitors), and the protein was washed with cation buffer and then with cation buffer containing 250 mM NaCl and eluted from the column with cation buffer containing 350 mM NaCl. This fraction was loaded onto a Ni^{2+}-Sepharose column (Amersham Biosciences HisTrap HP). The column was washed with imidazole buffer (50 mM phosphate buffer (pH 7.5), 300 mM NaCl, 10 mM imidazole, 10% glycerol, 1 mM $MgCl_2$, 20 μM ATP, and protease inhibitors) and then with imidazole buffer containing 70 mM imidazole, and the protein was eluted with imidazole buffer containing 300 mM imidazole. Peak fractions were pooled, aliquoted, and snap-frozen in liquid N_2. Protein was stored at −80 °C. XMAP215 was purified as described previously (24).

Porcine brain tubulin was purified as described previously (15). Cycled tubulin was labeled with Alexa Fluor 488 or rhodamine (TAMRA (5(6)-carboxytetramethylrhodamine succinimidyl ester), Invitrogen) as described by Hyman *et al.* (16). GMP-CPP[2]-stabilized microtubules were grown as described (17).

Budding yeast tubulin was purified from strain BJ2168. The culture was collected at an exponential phase of growth (A_{600} = 1), and the pellet was resuspended in buffer (0.7 ml of buffer/liter of cells) containing 30 mM HEPES (pH 7.2), 50 mM KOAc, 2 mM $Mg(OAc)_2$, 1 mM EGTA, 10% glycerol, 0.2% Triton X-100, 0.2 mM PMSF, 10 μg/ml pepstatin A, 10 μg/ml leupeptin, and 10 μg/ml aprotinin. The cells were then dropped into liquid nitrogen, giving cryo-beads. The beads were processed by grinding in a Retsch ZM 200 grinder, yielding a final powder lysate that was stored at −80 °C. This lysate was used for purification of tubulin with the TOG column as described previously (18).

Polymerization Assays and Imaging—Dynamic microtubule assays using rhodamine-labeled seeds and dynamic (Alexa Fluor 488-labeled or unlabeled) extensions were performed as described previously (19). The imaging buffer consisted of BRB80 (80 mM PIPES, 1 mM $MgCl_2$, 1 mM EGTA, pH 6.8) supplemented with 40 mM glucose, 40 μg/ml glucose oxidase, 16 μg/ml catalase, 0.1 mg/ml casein, 1% DTT, 1 mM GTP, and 50 mM KCl (unless stated otherwise). In total internal reflection fluorescence microscopy experiments, images were acquired every 5 or 10 s with an Andor iXon camera on a Zeiss inverted microscope with a Zeiss alpha FLUAR 100×/1.45 oil objective. An objective heater was used to heat the sample to 35 °C (brain tubulin) or 28 °C (yeast tubulin). Static assays were performed in the same way as the dynamic assays, except that Alexa Fluor 488-labeled tubulin was not used in this case, and GTP was not added to the imaging buffer. Images were collected either every 10 s or every 100 ms (in streaming mode). In differential interference contrast (DIC) experiments, we used the setup described previously (20). Data were analyzed by making kymographs from acquired images using Fiji software, which were then used to measure the parameters of microtubule dynamics. Growth rate was determined by measuring the change in length of a microtubule over time. Catastrophe frequency was expressed as the number of catastrophes over the total time of microtubule growth.

RESULTS

Stu2 Is a Weak Polymerase on Porcine Brain Tubulin—To investigate the activity of Stu2, we first performed experiments using porcine brain tubulin. Stable microtubules were grown from porcine brain tubulin, 25% of which was labeled with rhodamine, in the presence of GMP-CPP, a slowly hydrolyzable GTP analog (21). These stable microtubules were bound to the surface of a coverslip using anti-rhodamine antibodies and imaged by total internal reflection fluorescence microscopy (Fig. 1*A*). To investigate the effect of Stu2 on microtubule growth, 7 μM 10% Alexa Fluor 488-labeled porcine brain tubulin and various concentrations of unlabeled Stu2 were added. Microtubule growth and the transition between the growing and shrinking phases were quantified from the kymographs (Fig. 1*B*). Increasing the concentration of Stu2 increased the microtubule growth rate at the plus end by 2.4-fold from 0.448 ± 0.010 μm/min (mean ± S.E., n = 91) in control experiments with tubulin to only 1.071 ± 0.034 μm/min (mean ± S.E., n = 121) with 500 nM Stu2 (Fig. 1*C*, *left panel*). Approximately 200 nM Stu2 was required to reach 50% of this increase in growth rate. A similar acceleration of growth was observed at the minus end: Stu2 increased the growth rate from 0.131 ± 0.007 μm/min (mean ± S.E., n = 22) with tubulin alone to 0.342 ± 0.011 μm/min with 500 nM Stu2 (mean ± S.E., n = 79). Thus, Stu2 is a microtubule polymerase, like its *Xenopus* relative XMAP215 and its *Aspergillus* relative Tea1, although the acceleration of growth by Stu2 is only ~2-fold less than the 8-fold increase observed for the other proteins.

Stu2 had a small effect on catastrophe (Fig. 1*C*, *right panel*). In the absence of Stu2, the catastrophe rate at the plus end was 0.119 ± 0.013 min^{-1} (mean ± S.E., n = 79). This rate increased slightly but significantly at intermediate Stu2 concentrations

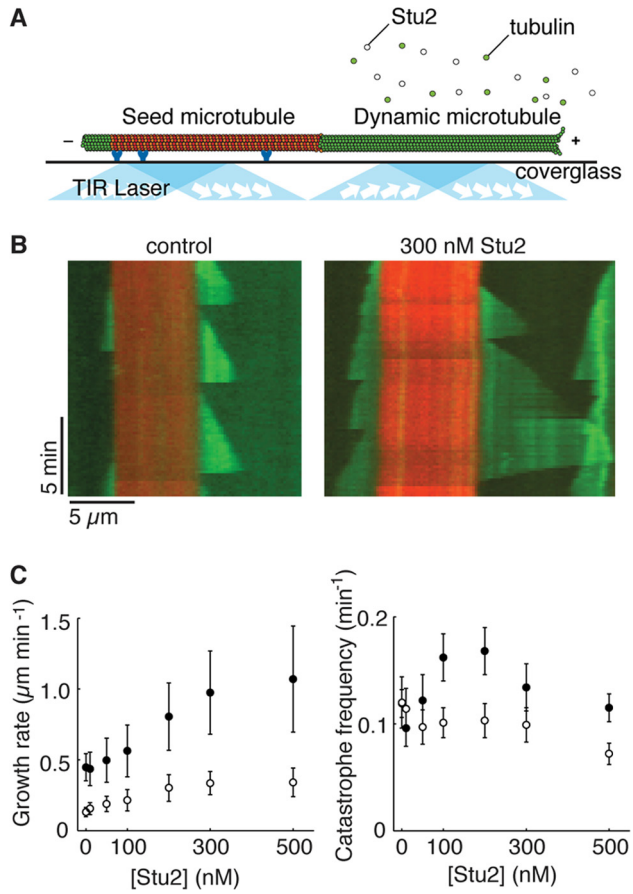

FIGURE 1. **Stu2 is a weak polymerase on porcine brain tubulin.** *A*, schematic of the experimental design. Alexa Fluor 488-labeled porcine brain tubulin (*green*) in solution polymerizes onto the ends of rhodamine-labeled GMP-CPP-stabilized microtubules (*red*) bound to the coverslip with anti-rhodamine antibodies (*blue*). The surface of the flow chamber is imaged using total internal reflection (*TIR*) fluorescence microscopy, which minimizes background from the fluorescent tubulin in solution. *B*, kymographs in the absence (*left*) and presence (*right*) of Stu2 (300 nM) show that Stu2 accelerates growth at both ends (7 μM tubulin, 35 °C, BRB80 + 50 mM KCl). *C*, dependence of rates of microtubule growth (*left*) and catastrophe (*right*) on Stu2 concentration. ●, plus end; ○, minus end. Data are means ± S.D. of 33–121 microtubules for the growth rate and means ± S.E. for the catastrophe rate, where the S.E./mean was set equal to the reciprocal of the square root of the number of catastrophes (between 33 and 78 for the various concentrations).

(0.162 ± 0.022 min^{-1} at 100 nM and 0.168 ± 0.022 min^{-1} at 200 nM) but then decreased to control levels at 500 nM. At the minus end, Stu2 slightly inhibited catastrophe. The effect of Stu2 was similar to that of XMAP215 and Tea 1, which increased catastrophe at the plus end by 2.6- and 2.7-fold, respectively, at 200 nM (8, 22). Based on these effects on the growth rate and catastrophe frequency (and assuming the model of Ref. 23), Stu2 is expected to increase the mean length at which microtubules catastrophe at the plus end from 3.8 μm (0 Stu2) to 8.9 μm (500 nM Stu2), similar to the measured values of 3.5 ± 0.4 μm (0 Stu2, mean ± S.E., $n = 79$) to 8.2 ± 0.9 μm (500 nM Stu2, mean ± S.E., $n = 78$).

Stu2 Binds to the Microtubule Ends and Acts as a Depolymerase in the Absence of Tubulin—We used a GFP-tagged construct to directly observe Stu2 interactions with microtubules. Stu2-GFP has a weak polymerase activity with porcine brain tubulin. The addition of 100 nM Stu2-GFP caused a modest increase in microtubule growth rate in 10 μM tubulin from 0.386 ± 0.050 μm/min (mean ± S.D., $n = 9$) to 0.485 ± 0.081 μm/min (mean ± S.D., $n = 20$). This rate increase was similar to that induced by the same concentration of unlabeled Stu2 (Fig. 1*C*). During dynamic assays in the presence of unlabeled tubulin, Stu2-GFP bound to the plus end of growing microtubules with higher affinity than the seed or the extension (Fig. 2*A*). At low concentrations of Stu2 ($\ll$1 nM), single molecules of Stu2-GFP were observed to bind to and diffuse on the microtubule surface; other Stu2 molecules were observed to bind stably near both microtubule ends (Fig. 2*B*). At lower salt concentrations, Stu2-GFP bound much more strongly to the microtubule lattice (Fig. 2*C*). In BRB80 without extra KCl, GMP-CPP-stabilized microtubules were decorated with Stu2-GFP along their whole length; furthermore, under these conditions, Stu2-GFP accelerated the depolymerization of these stable microtubules by 10-fold from the spontaneous rate of 0.0046 ± 0.0023 μm/min (mean ± S.D., $n = 18$) to 0.058 ± 0.014 μm/min (mean ± S.D., $n = 35$; $p < 0.0001$ by a *t* test).

At 7 μM porcine brain tubulin, no rescues were observed; in the presence of 500 nM Stu2, the rescue rate increased to 0.54 ± 0.09 min^{-1} (mean ± S.E., $n = 36$ rescues). However, rescues were still relatively infrequent. At 500 nM Stu2, only 46% of the

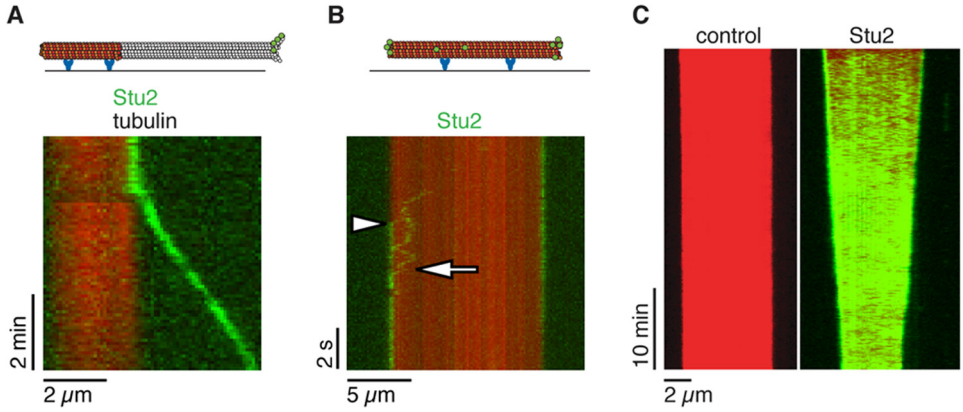

FIGURE 2. **Interaction of Stu2-GFP with porcine brain microtubules.** *A*, Stu2-GFP preferentially binds to the plus end of a growing microtubule (1.5 nM Stu2-GFP, 10 μM unlabeled tubulin, 35 °C, BRB80). *B*, Stu2-GFP (73 pM) can bind to the lattice and diffuse (*arrow*), or it can stably bind near one or both ends (*arrowhead*) (0 μM added tubulin, 35 °C, BRB80 + 110 mM KCl). *C*, Stu2-GFP depolymerizes GMP-CPP-stabilized microtubules in the absence of free tubulin in solution. In the absence of Stu2-GFP, the spontaneous depolymerization was not detectable over 30 min (*left panel*); in the presence of GFP-Stu2, the microtubules depolymerized (*right panel*) (58 pM Stu2-GFP, 0 μM added tubulin, 35 °C, BRB80).

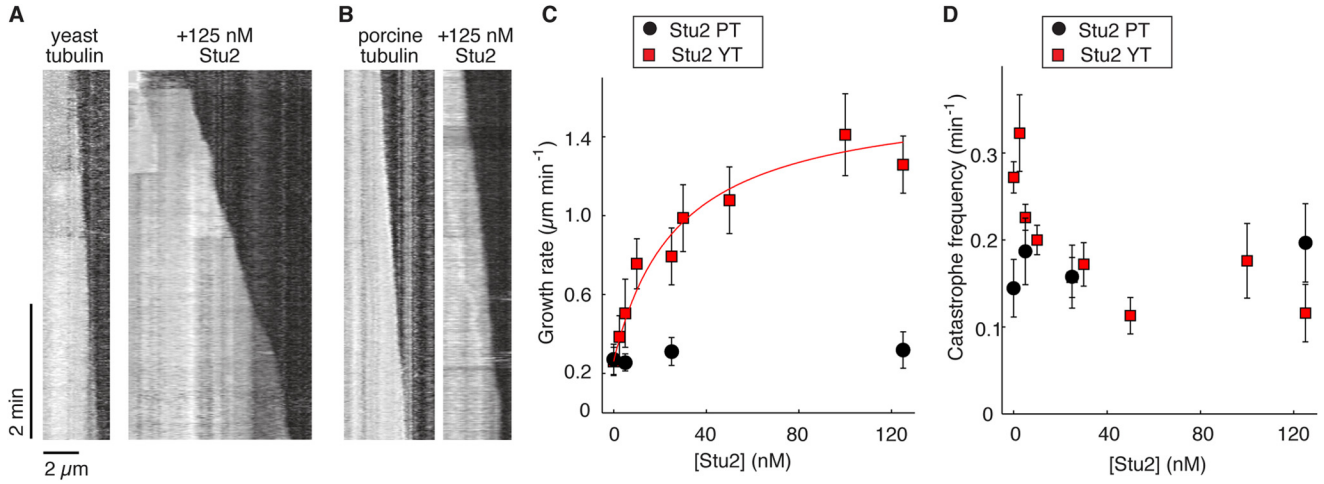

FIGURE 3. **Stu2 is a strong polymerase on budding yeast tubulin.** *A*, kymographs showing the effect of Stu2 on microtubule growth in the presence of budding yeast tubulin (DIC microscopy, 5 μM tubulin, 28 °C, BRB80 + 50 mM KCl). *B*, corresponding kymographs in the presence of unlabeled porcine brain microtubules (9 μM tubulin, 28 °C, BRB80 + 50 mM KCl). *C*, Stu2 accelerates the polymerization of yeast tubulin (*YT*; *red squares*) to a greater extent than porcine brain tubulin (*PT*; *black circles*). Data points are means ± S.D. For yeast tubulin, $n = 198$ microtubules in the absence of Stu2, and $n = 37$–157 microtubules in the presence of Stu2. For porcine tubulin, $n = 29$ microtubules in the absence of Stu2 and $n = 13$–20 microtubules in the presence of Stu2. The *red line* is the fit to the Michaelis-Menten equation ($K_m = 22.7 \pm 5.5$ nM and $V_{max} = 1.51 \pm 0.10$ μm/min (mean ± S.E.); $V_0 = 0.26 \pm 0.07$ μm/min (mean ± S.D.)). *D*, Stu2 decreases the catastrophe frequency of yeast microtubules. Data points are means ± S.E., where the S.E. was calculated as the mean divided by the square root of the number of catastrophes, which ranged from 12 to 240.

shrinking plus ends rescued; this is expected to increase the microtubule length at catastrophe by a factor of <2.

Stu2 Is a Strong Polymerase on Budding Yeast Tubulin—After characterizing the interaction of Stu2 with porcine brain tubulin, we studied its interaction with the conspecific budding yeast tubulin purified from strain BJ2168 (see "Experimental Procedures"). Because the yield was low (18), we had insufficient protein for fluorescent labeling. We therefore used DIC microscopy to visualize the microtubules extending from GMP-CPP-stabilized porcine tubulin seeds. We made two other changes in the assays conditions. First, we performed the experiments at 28 °C, which is more appropriate for physiological conditions of budding yeast proteins. Second, we used a lower concentration of yeast tubulin than brain tubulin because yeast tubulin polymerizes at lower concentrations than mammalian tubulin, as reported previously (25, 26).

Stu2 increased the elongation rate of microtubules grown in 5 μM yeast tubulin by 5-fold from 0.26 ± 0.04 μm/min (mean ± S.D., $n = 36$) to 1.26 ± 0.14 μm/min (mean ± S.D., $n = 37$) in the presence of 125 nM Stu2 (Fig. 3, *A* and *C*). The Michaelis-Menten fit to these data gave a K_m of 22.7 ± 5.5 nM (mean ± S.E.) and a V_{max} of 1.51 ± 0.10 μm/min (mean ± S.E.). Thus, Stu2 accelerated growth in yeast tubulin to a greater degree than in porcine brain tubulin. Furthermore, this acceleration of growth occurred at much lower Stu2 concentrations, 23 nM for half-maximal acceleration for yeast tubulin compared with ~200 nM for mammalian tubulin. For example, 5 nM Stu2 was sufficient to double the growth rate of yeast microtubules, whereas nearly 500 nM Stu2 was needed to double the growth rate of porcine microtubules (Fig. 1). There was also a difference between yeast and mammalian tubulins at tubulin concentrations that gave the same basal growth rates. At 9 μM porcine tubulin, 125 nM Stu2 increased the growth rate by only 20% from 0.27 ± 0.08 μm/min (mean ± S.D., $n = 29$) to 0.32 ± 0.09 μm/min (mean ± S.D., $n = 13$) (Fig. 3, *B* and *C*). By comparison, 125 nM Stu2 increased the growth rate of yeast tubulin by 470% to 1.23 ± 0.15 μm/min (mean ± S.D., $n = 37$).

In addition to increasing growth rate, Stu2 also decreased the catastrophe frequency of yeast microtubules (Fig. 3*D*). In the absence of Stu2, the catastrophe frequency was 0.272 ± 0.018 min^{-1} (mean ± S.E., $n = 240$ catastrophes), and this rate decreased to 0.116 ± 0.033 min^{-1} (mean ± S.E., $n = 12$ catastrophes) in the presence of 125 nM Stu2. Based on these effects on the growth rate and catastrophe frequency (and again assuming the model of Ref. 23), Stu2 is expected to increase the mean length at which yeast microtubules undergo catastrophe at the plus end from 0.96 μm (0 Stu2) to 10.8 μm (125 nM Stu2), similar to the measured values of 1.3 ± 0.2 μm (0 Stu2, mean ± S.E., $n = 28$) and 11.5 ± 3.3 μm (125 nM Stu2, mean ± S.E., $n = 12$). Thus, Stu2 promotes the growth of yeast microtubules, increasing mean length by 10-fold through its combination of polymerase and anti-catastrophe activities. No rescues were observed.

XMAP215 Is a Strong Polymerase of Yeast Tubulin—Having found that Stu2 is a strong polymerase of its conspecific tubulin, we asked whether XMAP215 is also a stronger polymerase of vertebrate tubulin over yeast tubulin. To the contrary, we found that XMAP215 is also a strong polymerase of yeast tubulin. When we introduced increasing amounts of XMAP215 and 5 μM budding yeast tubulin to GMP-CPP-stabilized seeds and visualized the formation of dynamic microtubules using DIC microscopy at 28 °C (Fig. 4, *A* and *B*), we observed a large increase in yeast microtubule growth rates. Namely, the growth rate increased by 13-fold from 0.26 ± 0.07 μm/min (mean ± S.D., $n = 198$) observed with yeast tubulin alone to 3.45 ± 0.87 μm/min (mean ± S.D., $n = 45$) in the presence of 125 nM XMAP215. Consistent with previous reports (22, 24), XMAP215 caused an 9-fold increase in porcine microtubule growth rates, increasing the growth rate from 0.32 ± 0.08 μm/min (mean ± S.D., $n = 106$) in the absence of XMAP215 to

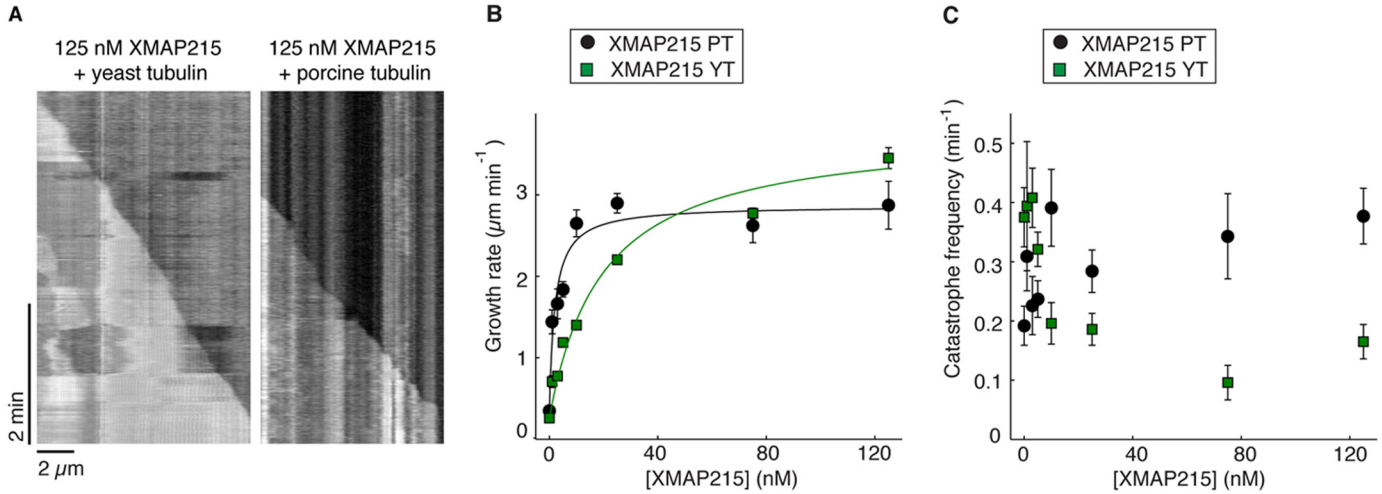

FIGURE 4. **Effects of XMAP215 on the dynamics of porcine and yeast tubulins.** *A*, kymographs showing the effect of XMAP215 on porcine and yeast microtubules (DIC microscopy, 5 μM yeast tubulin and 9 μM porcine tubulin with 125 nM XMAP215, 28 °C, BRB80 + 50 mM KCl). *B*, XMAP215 promotes the polymerization of budding yeast tubulin (*green squares*) to a similar extent as porcine brain tubulin (*black circles*). Data points are means ± S.E. For porcine tubulin, $n = 106$ microtubules in the absence of XMAP215, and $n = 14–116$ microtubules in the presence of XMAP215. For yeast tubulin, $n = 198$ microtubules in the absence of XMAP215 and $n = 9–123$ microtubules in the presence of XMAP215. *Black* and *green lines* are the fits to the Michaelis-Menten equation (K_m = 2.13 ± 0.56 nM and K_m = 17.35 ± 3.22 nM for porcine and yeast tubulins, respectively (mean ± S.E.); V_{max} = 2.88 ± 0.56 and 3.64 ± 0.20 μm/min for porcine and yeast tubulins, respectively (mean ± S.E.); V_0 = 0.32 ± 0.08 and 0.26 ± 0.07 μm/min for porcine and yeast tubulins, respectively (mean ± S.D.)). *C*, XMAP215 decreases the catastrophe frequency of yeast tubulin but increases the catastrophe of porcine tubulin. Data points are means ± S.E., where the S.E. was calculated as the mean divided by the square root of the number of catastrophes, which ranged from 19 to 66 for pig tubulin experiments and from 11 to 119 for yeast tubulin experiments.

2.87 ± 1.25 μm/min (mean ± S.D., $n = 18$) in the presence of 125 nM XMAP215. These results show that XMAP215 increases the polymerization rates of both yeast and porcine tubulins to similar extents. However, the Michaelis-Menten fits to these curves reveal different K_m values, indicating that XMAP215 is more active on porcine tubulin than on yeast tubulin (K_m for porcine brain tubulin = 2.13 ± 0.56 nM, which is considerably lower than that for yeast tubulin, K_m = 17.35 ± 3.22 nM).

XMAP215 doubled the catastrophe frequency of porcine microtubules from 0.192 ± 0.033 min^{-1} (mean ± S.E., $n = 33$) in the control experiment to 0.377 ± 0.047 min^{-1} (mean ± S.E., $n = 66$) in the presence of 125 nM XMAP215 (Fig. 4*C*). In contrast, when yeast tubulin was used, the addition of 125 nM XMAP215 halved the catastrophe frequency from 0.375 ± 0.050 min^{-1} (mean ± S.E., $n = 56$) to 0.165 ± 0.029 min^{-1} (mean ± S.E., $n = 32$). No rescues were observed with or without XMAP215.

DISCUSSION

We found that Stu2 stimulates the growth of microtubules polymerizing in the presence of budding yeast tubulin. The maximum stimulation of 5-fold is similar to that of the evolutionarily related proteins XMAP215 and Tea1. Thus, Stu2 is a microtubule polymerase, like the other members of the XMAP215/Dis1 family. The polymerase activity of purified Stu2 occurs at concentrations similar to those found in cells (80 nM) (27) and accounts for some of the observed phenotypes during mitosis. For example, anaphase microtubule elongation is impaired in both Stu2-depleted and Stu2-ΔTOG1 mutant cells (9–11), as expected if polymerase activity is decreased. The effects of Stu2 depletion on the dynamics of cytoplasmic microtubules (10) are not easily reconciled with our *in vitro* results, suggesting that interactions of Stu2 with other MAPs may be involved.

We could not confirm earlier results showing that Stu2 inhibits, rather than promotes, elongation of mammalian brain microtubules (12). Although Stu2 is a weak polymerase in the presence of porcine brain tubulin and requires high Stu2 concentrations, it nevertheless promoted microtubule growth under all conditions that we tested.

A key finding was that Stu2 has higher polymerase activity on budding yeast tubulin than on porcine brain tubulin. Although the α- and β-tubulins are highly evolutionarily conserved families of proteins, there are considerable differences between budding yeast and mammalian tubulins at both the gene and protein levels that might lead to this difference in Stu2 activity. Budding yeast has two α-tubulin genes and one β-tubulin gene (28, 29), whereas vertebrates have six α-tubulin genes and seven β-tubulin genes (30). Within α- and β-tubulins, the sequence identity between yeast and mammalian proteins is only 70–75%, with large differences at their C termini. Post-translational modifications of vertebrate tubulins lead to additional tubulin complexity at the protein level (31). These post-translational modifications occur mostly on the C termini of α- and β-tubulins, sites that are recognized by many regulators of microtubule dynamics (31, 32), including XMAP215 (24). In the case of bovine brain tubulin, these different gene products and post-translational modifications give rise to up to 21 different tubulin species that are distinguishable on an isoelectric focusing gel (33, 34) Thus, there are many potential molecular mechanisms that could give rise to the differences in activity of Stu2 on the different sources of tubulin.

XMAP215 also differentiated between tubulins: although the maximum enhancement of growth was in the same range for

yeast and porcine tubulins, less XMAP215 was needed to give a half-maximal promotion on porcine tubulin compared with yeast tubulin. This provides additional evidence for differences between yeast and brain tubulins. The lower concentration of XMAP215 required to accelerate growth may reflect a higher affinity of XMAP215 for the end of porcine microtubules; once at the end, however, the growth acceleration is similar. Interestingly, under the conditions that we tested, XMAP215 was a stronger polymerase than Stu2 on both tubulins, enhancing the growth rates of yeast and porcine tubulins by 13- and 9-fold, respectively, compared with enhancements of 5- and 2-fold by Stu2.

Stu2 decreased the catastrophe frequency of yeast microtubules but had little effect on the catastrophe frequency of porcine microtubules. Interestingly, XMAP215 also decreased catastrophe in yeast tubulin but increased catastrophe in porcine tubulin. This is another difference in regulation by MAPs between yeast and porcine tubulins. It is possible that these effects reflect the inherent differences in polymerization dynamics of these two tubulin types.

Stu2 shares many properties with XMAP215. Both accelerate microtubule growth and inhibit catastrophe, both preferentially bind microtubule ends over lattice, both diffuse on the lattice, and both accelerate depolymerization of stable microtubules when there is no free tubulin in solution. There are, however, some differences. As reported above, Stu2 can bind to the minus end, where it accelerates microtubule growth, which is not observed for XMAP215 (24). Another possible difference between Stu2 and XMAP215 is that the former increased the rate of transition from shrinking to growing (rescue). By contrast, rescues have not been reported for XMAP215 (and we also saw no rescues under our experimental conditions).

In summary, our results demonstrate that differences between yeast and mammalian tubulins can give rise to differential activities of interacting proteins, such as previously reported for kinesin (35) and dynein (36). In this study, we reported significant differences in protein activity when using tubulins from different sources, showing the importance of using conspecific tubulin when studying MAPs.

Acknowledgments—We thank S. Gandhi for cloning Stu2 constructs; D. Drechsel for advice and support; R. Lührmann, B. Kastner, T. Conrad, and N. Rigo for help with growing the large-scale budding yeast culture; A. Hyman, I. Tolic, and M. Zanic for useful discussions; and all members of the Howard laboratory for comments on this manuscript.

REFERENCES

1. Howard, J. (2001) *Mechanics of Motor Proteins and the Cytoskeleton*, Sinauer Associates, Inc., Publishers, Sunderland, MA
2. Cassimeris, L., and Tran, P. T. (eds) (2010) *Microtubules: In Vivo*, 1st Ed., Academic Press, New York
3. Howard, J., and Hyman, A. A. (2007) Microtubule polymerases and depolymerases. *Curr. Opin. Cell Biol.* **19,** 31–35
4. Akhmanova, A., and Steinmetz, M. O. (2008) Tracking the ends: a dynamic protein network controls the fate of microtubule tips. *Nat. Rev. Mol. Cell Biol.* **9,** 309–322
5. van der Vaart, B., Akhmanova, A., and Straube, A. (2009) Regulation of microtubule dynamic instability. *Biochem. Soc. Trans.* **37,** 1007–1013
6. Al-Bassam, J., and Chang, F. (2011) Regulation of microtubule dynamics by TOG-domain proteins XMAP215/Dis1 and CLASP. *Trends Cell Biol.* **21,** 604–614
7. Gard, D. L., and Kirschner, M. W. (1987) A microtubule-associated protein from *Xenopus* eggs that specifically promotes assembly at the plus end. *J. Cell Biol.* **105,** 2203–2215
8. Takeshita, N., Mania, D., Herrero, S., Ishitsuka, Y., Nienhaus, G. U., Podolski, M., Howard, J., and Fischer, R. (2013) The cell-end marker TeaA and the microtubule polymerase AlpA contribute to microtubule guidance at the hyphal tip cortex of *Aspergillus nidulans* to provide polarity maintenance. *J. Cell Sci.* **126,** 5400–5411
9. Severin, F., Habermann, B., Huffaker, T., and Hyman, T. (2001) Stu2 promotes mitotic spindle elongation in anaphase. *J. Cell Biol.* **153,** 435–442
10. Kosco, K. A., Pearson, C. G., Maddox, P. S., Wang, P. J., Adams, I. R., Salmon, E. D., Bloom, K., and Huffaker, T. C. (2001) Control of microtubule dynamics by Stu2p is essential for spindle orientation and metaphase chromosome alignment in yeast. *Mol. Biol. Cell* **12,** 2870–2880
11. Al-Bassam, J., van Breugel, M., Harrison, S. C., and Hyman, A. (2006) Stu2p binds tubulin and undergoes an open-to-closed conformational change. *J. Cell Biol.* **172,** 1009–1022
12. van Breugel, M., Drechsel, D., and Hyman, A. (2003) Stu2p, the budding yeast member of the conserved Dis1/XMAP215 family of microtubule-associated proteins is a plus end-binding microtubule destabilizer. *J. Cell Biol.* **161,** 359–369
13. Ayaz, P., Ye, X., Huddleston, P., Brautigam, C. A., and Rice, L. M. (2012) A TOG:$\alpha\beta$-tubulin complex structure reveals conformation-based mechanisms for a microtubule polymerase. *Science* **337,** 857–860
14. Widlund, P. O., Stear, J. H., Pozniakovsky, A., Zanic, M., Reber, S., Brouhard, G. J., Hyman, A. A., and Howard, J. (2011) XMAP215 polymerase activity is built by combining multiple tubulin-binding TOG domains and a basic lattice-binding region. *Proc. Natl. Acad. Sci. U.S.A.* **108,** 2741–2746
15. Gell, C., Friel, C. T., Borgonovo, B., Drechsel, D. N., Hyman, A. A., and Howard, J. (2011) Purification of tubulin from porcine brain. *Methods Mol. Biol.* **777,** 15–28
16. Hyman, A., Drechsel, D., Kellogg, D., Salser, S., Sawin, K., Steffen, P., Wordeman, L., and Mitchison, T. (1991) Preparation of modified tubulins. *Methods Enzymol.* **196,** 478–485
17. Hunter, A. W., Caplow, M., Coy, D. L., Hancock, W. O., Diez, S., Wordeman, L., and Howard, J. (2003) The kinesin-related protein MCAK is a microtubule depolymerase that forms an ATP-hydrolyzing complex at microtubule ends. *Mol. Cell* **11,** 445–457
18. Widlund, P. O., Podolski, M., Reber, S., Alper, J., Storch, M., Hyman, A. A., Howard, J., and Drechsel, D. N. (2012) One-step purification of assembly-competent tubulin from diverse eukaryotic sources. *Mol. Biol. Cell* **23,** 4393–4401
19. Gell, C., Bormuth, V., Brouhard, G. J., Cohen, D. N., Diez, S., Friel, C. T., Helenius, J., Nitzsche, B., Petzold, H., Ribbe, J., Schäffer, E., Stear, J. H., Trushko, A., Varga, V., Widlund, P. O., Zanic, M., and Howard, J. (2010) Microtubule dynamics reconstituted in vitro and imaged by single-molecule fluorescence microscopy. *Methods Cell Biol.* **95,** 221–245
20. Bormuth, V., Howard, J., and Schäffer, E. (2007) LED illumination for video-enhanced DIC imaging of single microtubules. *J. Microsc.* **226,** 1–5
21. Hyman, A. A., Salser, S., Drechsel, D. N., Unwin, N., and Mitchison, T. J. (1992) Role of GTP hydrolysis in microtubule dynamics: information from a slowly hydrolyzable analogue, GMP-CPP. *Mol. Biol. Cell* **3,** 1155–1167
22. Zanic, M., Widlund, P. O., Hyman, A. A., and Howard, J. (2013) Synergy between XMAP215 and EB1 increases microtubule growth rates to physiological levels. *Nat. Cell Biol.* **15,** 688–693
23. Verde, F., Dogterom, M., Stelzer, E., Karsenti, E., and Leibler, S. (1992) Control of microtubule dynamics and length by cyclin A- and cyclin B-dependent kinases in *Xenopus* egg extracts. *J. Cell Biol.* **118,** 1097–1108
24. Brouhard, G. J., Stear, J. H., Noetzel, T. L., Al-Bassam, J., Kinoshita, K., Harrison, S. C., Howard, J., and Hyman, A. A. (2008) XMAP215 is a processive microtubule polymerase. *Cell* **132,** 79–88
25. Davis, A., Sage, C. R., Wilson, L., and Farrell, K. W. (1993) Purification and biochemical characterization of tubulin from the budding yeast *Saccharomyces cerevisiae*. *Biochemistry* **32,** 8823–8835
26. Barnes, G., Louie, K. A., and Botstein, D. (1992) Yeast proteins associated

with microtubules *in vitro* and *in vivo*. *Mol. Biol. Cell* **3,** 29–47
27. Ghaemmaghami, S., Huh, W.-K., Bower, K., Howson, R. W., Belle, A., Dephoure, N., O'Shea, E. K., and Weissman, J. S. (2003) Global analysis of protein expression in yeast. *Nature* **425,** 737–741
28. Neff, N. F., Thomas, J. H., Grisafi, P., and Botstein, D. (1983) Isolation of the β-tubulin gene from yeast and demonstration of its essential function *in vivo*. *Cell* **33,** 211–219
29. Schatz, P. J., Pillus, L., Grisafi, P., Solomon, F., and Botstein, D. (1986) Two functional α-tubulin genes of the yeast *Saccharomyces cerevisiae* encode divergent proteins. *Mol. Cell Biol.* **6,** 3711–3721
30. Ludueña, R. F. (1998) Multiple forms of tubulin: different gene products and covalent modifications. *Int. Rev. Cytol.* **178,** 207–275
31. Janke, C., and Bulinski, J. C. (2011) Post-translational regulation of the microtubule cytoskeleton: mechanisms and functions. *Nat. Rev. Mol. Cell Biol.* **12,** 773–786
32. Sirajuddin, M., Rice, L. M., and Vale, R. D. (2014) Regulation of microtubule motors by tubulin isotypes and post-translational modifications. *Nat. Cell Biol.* **16,** 335–344
33. Williams, R. C., Jr., Shah, C., and Sackett, D. (1999) Separation of tubulin isoforms by isoelectric focusing in immobilized pH gradient gels. *Anal. Biochem.* **275,** 265–267
34. Field, D. J., Collins, R. A., and Lee, J. C. (1984) Heterogeneity of vertebrate brain tubulins. *Proc. Natl. Acad. Sci. U.S.A.* **81,** 4041–4045
35. Alonso, M. C., Drummond, D. R., Kain, S., Hoeng, J., Amos, L., and Cross, R. A. (2007) An ATP gate controls tubulin binding by the tethered head of kinesin-1. *Science* **316,** 120–123
36. Alper, J. D., Tovar, M., and Howard, J. (2013) Displacement-weighted velocity analysis of gliding assays reveals that *Chlamydomonas* axonemal dynein preferentially moves conspecific microtubules. *Biophys. J.* **104,** 1989–1998